

# Charge Separation at Interfaces of Phase-Separated Coacervates

Arghya Majee,<sup>1</sup> Christoph A. Weber,<sup>2,\*</sup> and Frank Jülicher<sup>1,3,4,\*</sup>

<sup>1</sup>Max Planck Institute for the Physics of Complex Systems, 01187 Dresden, Germany

<sup>2</sup>Faculty of Mathematics, Natural Sciences, and Materials Engineering: Institute of Physics, University of Augsburg, Universitätsstr. 1, 86159 Augsburg, Germany

<sup>3</sup>Center for Systems Biology Dresden, 01307 Dresden, Germany

<sup>4</sup>Cluster of Excellence Physics of Life, TU Dresden, 01062 Dresden, Germany

(Dated: October 11, 2023)

We present a theory for phase-separated liquid coacervates with salt, taking into account spatial heterogeneities and interfacial profiles. We find that charged layers of alternating sign can form around the interface while the bulk phases remain approximately charge-neutral. We show that the salt concentration regulates the number of layers and the amplitude of the layer's charge density and electrostatic potential. Such charged layers can either repel or attract single-charged molecules diffusing across the interface. Our theory could be relevant for artificial systems and biomolecular condensates in cells. Our work suggests that interfaces of biomolecular condensates could mediate charge-specific transport similar to membrane-bound compartments.

## I. INTRODUCTION

Spatial organization of macromolecules is essential for regulating cellular processes. Most biochemical processes involve charged macromolecules like DNA, RNA, and proteins, that are immersed in a multi-component, aqueous electrolyte solution containing various salt ions. These biomolecules assemble into specific compartments that provide unique environments to perform certain tasks [1, 2]. Moreover, compartmentalization of prebiotic components and chemical reactions was also proposed as a selection mechanism at the origin of life [3–6].

Compartments in cells can either be membrane-bound, or membrane-less liquid droplets that can disperse and reform for varying conditions in cells [7–9]. Such intracellular droplets are called biomolecular condensates and often form via liquid-liquid phase separation [1, 2, 10, 11]. Many biomolecular condensates in cells contain negatively charged RNA and positively charged proteins [12] suggesting coacervation as a mechanism underlying their formation [13]. Indeed, in vitro experiments show that condensate properties are strongly affected by salt concentration [14–16]. Coacervates are liquid droplets composed of charged macromolecules and counterions interacting via electrostatic interactions. In physical chemistry, they are classified into two categories [17]: *simple* coacervates formed by a single type of macroion and its counterions, and *complex* coacervates due to electrostatic interactions between oppositely charged macroions. Coacervation as a mechanism to spatially organize and select molecules was already proposed at the beginning of the twentieth century as an organizing principle for the molecular origin of life [3, 4].

A first theoretical model for coacervates was proposed by Voorn-Overbeek [18]. Within this model, phase separation results from a competition between the mixing

entropy and the electrostatic interactions between the oppositely charged molecules, which is described using the Debye-Hückel approximation in the Poisson-Boltzmann equation treating ions as dilute components. However, when coacervates form, charged macromolecules and salt ions are in general non-dilute and interactions among all charged components are essential, in particular at physiological conditions. Interactions were shown to indeed affect the distribution of macroions close to charged surfaces [19, 20]. Most theories on electrolytes study flat and colloidal charged surfaces that are solid [21, 22]. In contrast, coacervates provide phase boundaries separating liquid phases that are soft and permeable. So far, this scenario has not been explored.

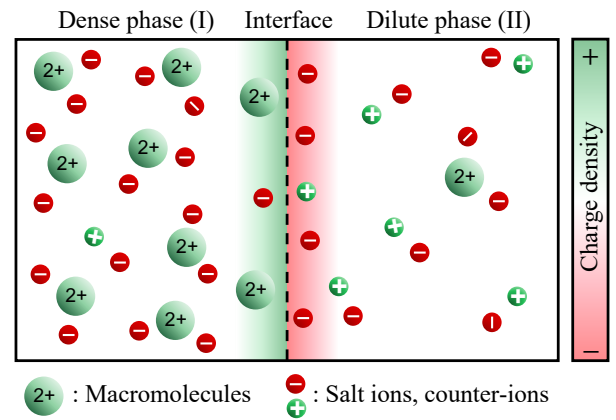


FIG. 1. **Schematics of the considered phase-separated electrolyte mixtures.** Macromolecule-rich phases (phase I) can form in an initially homogeneous saline solution with macromolecules (big green circles). Macromolecules are depicted to be positively charged with counter ions being anions. Dissociation of salts also generate co/counter-ions. Charges can separate with a charge density that deviates from electro-neutrality, in particular around the interface (indicated by the color gradients).

\* corresponding authors: christoph.weber@physik.uni-augsburg.de and julicher@pks.mpg.de

Recent experimental studies show that coacervate phase boundaries give rise to rich physical behavior [14, 23–27]. Condensates can carry a surface charge and thus move in an applied electric field due to electrophoresis [24, 26, 27]. The surface charge and the associated zeta potential were also recognized as one of the factors determining droplet stability [26]. Not only that, the interfacial tension of protein droplets depends on salinity as well as on the Donnan potential difference that exists between two coexisting phases [14, 28]. Such studies indeed highlight the importance of electrostatics and interfaces in phase-separated, coacervate systems. However, the thermodynamic mechanisms underlying the interfacial charge and the behavior of the electrostatic potential across coacervate phase boundaries remain unclear.

In this work, we present a theoretical framework for non-dilute mixtures composed of charged macromolecules and salt ions capable of forming coexisting phases, i.e., a coacervate phase-separated from a dilute phase. We account for the mean-field electrostatic interactions among all charged components and study the concentration profiles of components in each phase and in the interfacial domain. Our key finding is that charge separation occurs at interface while each phase is approximately charge-neutral (see an illustration in Fig. 1). The corresponding electrostatic potential shows a non-monotonic behavior with attractive wells and repulsive barriers. Strikingly, the electrostatic potential can also give rise to multiple layers of alternating charges. This implies that charged molecules may exhibit a complex transition kinetics through coacervate interfaces.

## II. ELECTROTHERMODYNAMICS OF PHASE SEPARATION

We consider an electrolyte mixture composed of charged macromolecules and counter-ions that can phase separate into a macromolecule-rich and a macromolecule-poor phase; see Fig. 1 for an illustration. Each component,  $i = 1, \dots, M$ , can carry a molecular charge  $q_i e$  with  $e$  denoting the positive elementary charge. Here we consider constant charge for each component and for simplicity do not account for chemical processes leading to charge regulation [29, 30]. Moreover, the electrolyte mixture is considered to be incompressible corresponding to constant molecular volumes  $\nu_i$ . Incompressibility implies that the condition  $\sum_{i=1}^M \nu_i n_i(\mathbf{x}) = 1$  holds locally, where  $n_i(\mathbf{x})$  denotes the concentration field of component  $i$  at position  $\mathbf{x}$ . At constant temperature and pressure, this condition reduces the thermodynamic description to  $(M - 1)$  independent concentration fields  $n_i(\mathbf{x})$ .

All the components in the mixture collectively generate a dielectric medium with permittivity  $\varepsilon = \varepsilon_r \varepsilon_0$ , where  $\varepsilon_0$  is the vacuum permittivity and  $\varepsilon_r$  denotes the relative permittivity which in general depends on composition  $\{n_i\}$ . The distributions of charges give rise to an electrostatic potential  $\psi(\mathbf{x})$ , which is related to the concentrations

$n_i(\mathbf{x})$  via the Poisson equation:

$$\nabla \cdot (\varepsilon \nabla \psi) = -\rho, \quad (1a)$$

where  $\rho(\mathbf{x}) = \sum_i q_i e n_i(\mathbf{x})$  is the local charge density.

The electrothermodynamics of the mixture is governed by the free energy functional

$$F[n_i, \psi] = \int d^3x \left[ f(n_i) + \sum_i \frac{\kappa_i}{2} (\nabla n_i)^2 + \frac{\varepsilon}{2} (\nabla \psi)^2 + \lambda \left( \nabla \cdot (\varepsilon \nabla \psi) + \rho \right) + \sum_i \mu_i^{\text{el}} \left( n_i - \frac{N_i}{V} \right) \right], \quad (1b)$$

where  $f$  is the free energy density. Moreover,  $\kappa_i$  is related to the interfacial tension characterizing the energy contribution due to the spatial gradients of the components in the system. We refer to  $\kappa_i$  as the gradient cost for component  $i$  in the following. We have neglected cross terms of the form  $\nabla n_i \cdot \nabla n_j$  for simplicity. The term proportional to  $(\nabla \psi)^2$  describes the electrostatic energy density arising from the charged components in the system. Moreover,  $\lambda$  is the Lagrange multiplier to impose that the Poisson Eq. (1a) is satisfied and  $\mu_i^{\text{el}}$  is the Lagrange multiplier fixing the total number of particles  $N_i = \int_V d^3x n_i(\mathbf{x})$  for each component  $i$  with  $V$  denoting the volume of the system.

To describe interactions among all components we choose the Flory-Huggins free energy density

$$\frac{f(n_i)}{k_B T} = \sum_{i=1}^M (n_i \ln(\nu_i n_i) + \omega_i n_i) + \sum_{j=2}^M \sum_{i=1}^{j-1} \chi_{ij} n_i n_j \quad (1c)$$

containing the mixing entropy, the internal free energies  $\omega_i$  and the mean field interactions among the charged components of interaction strength  $\chi_{ij}$ .

Thermodynamic equilibrium states are characterized by  $\delta F / \delta n_i = 0$  and  $\delta F / \delta \psi = 0$  leading to

$$\mu_i^{\text{el}} = \frac{\partial f}{\partial n_i} - \kappa_i \nabla^2 n_i + q_i e \psi - \frac{1}{2} \frac{\partial \varepsilon}{\partial n_i} (\nabla \psi)^2, \quad (1d)$$

$$\lambda = \psi. \quad (1e)$$

Here, the constant  $\mu_i^{\text{el}}$  is the exchange electrochemical potential and the Lagrange multiplier for the Poisson equation is the electrostatic potential  $\psi$ . When phases coexist, the value of  $\mu_i^{\text{el}}$  corresponds to the slope of the Maxwell construction and the osmotic pressures balance between the phases.

To solve the governing equations (i.e., the Poisson equation and the equations provided by constant exchange electrochemical potential conditions in Eq. (1d)), we use van Neumann boundary conditions for the electrostatic potential and the concentrations:

$$(\nabla \psi \cdot \mathbf{n})|_{\partial \Omega} = 0, \quad (1f)$$

$$(\nabla n_i \cdot \mathbf{n})|_{\partial \Omega} = 0, \quad (1g)$$

where  $\mathbf{n}$  is the unit outward normal to the system boundary  $\partial\Omega$  enclosing the system volume  $V$ . The van Neumann boundary condition for the electrostatic potential ensures that the electric field normal to the boundaries vanishes corresponding to zero surface charge. Integrating the Poisson Eq. (1a) over the system volume  $V$  using the boundary condition (1f) leads to overall electroneutral systems with  $\int d^3x \rho(\mathbf{x}) = 0$ . Note that we do not impose electroneutrality locally, i.e.,  $\rho(\mathbf{x}) \neq 0$  in general. The Neumann boundary condition for the concentration field corresponds to an inert boundary that has no affinity to adhere or repel components.

In summary, Eqs. (1) govern the position-dependent electrothermodynamics of a non-dilute mixture composed of charged components where a dense coacervate phase can coexist with a dilute phase. This theoretical framework extends the classical Poisson-Boltzmann theory [22] to non-dilute conditions where interactions among the charged components affect the electrostatic potential.

### III. RESULTS

In this work, we use our theoretical framework given by Eqs. (1) to study simple coacervates (Sect. III A) and complex coacervates (Sect. III B). For simplicity, we consider flat interfaces and a one dimensional system with a position  $x$ . We determine the position-dependent electrostatic potential  $\psi(x)$  together with concentration fields  $n_i(x)$  of all the different charged components. In all studies, we use a relative solvent permittivity  $\epsilon_r = 80$  corresponding to pure water, and a solvent molecular volume  $\nu_s = 0.03 \text{ nm}^3$ . When salt ions or counter-ions are present in the system, their molecular volumes are for simplicity equal to the solvent. The internal free energies  $\omega_i$  do not affect the results as they can be absorbed into the Lagrange multipliers  $\mu_i^{\text{el}}$ . In our studies on simple coacervates, we choose macromolecules carrying a positive charge. In general, macromolecules such as proteins can be positively or negatively charged under physiological conditions. This diversity arises because for example the human cytosol has a  $\text{pH} \simeq 7.2$  [31] and the human proteome shows a bimodal distribution with two major peaks located at  $\text{pI} \simeq 6.0$  and  $8.25$  [32].

#### A. Simple coacervates

##### 1. Minimal model for simple coacervates

We first discuss a minimal model for a simple coacervate that contains a single type of charged macromolecule ( $p$ ), a neutralizing counterion ( $-$ ), and a solvent component ( $s$ ). Phase separation in such a system takes place for sufficiently large and positive interaction parameters  $\chi_{ps}$ . For the numerical examples discussed below, we use  $\chi_{ps} = 1.5 \text{ nm}^{-3}$  together with  $\chi_{-s} = -0.09 \text{ nm}^{-3}$ ,  $\chi_{p-} = -1.0 \text{ nm}^{-3}$ , and the volume

ratios  $\nu_p/\nu_s = \nu_p/\nu_- = 20$ . The counterions are assumed to be monovalent, e.g.,  $\text{OH}^-$ , with  $q_- = -1$ , and the macromolecule has a charge  $q_p = +3$  if not stated otherwise. For such parameters, we numerically solved Eqs. (1).

Coexistence of a dense coacervate phase and a dilute phase is reflected in the concentration profiles of charged components  $n_i(x)$  which are depicted in Fig. 2(a) for different  $\kappa_p/\kappa_-$  ratios. Both charged components show a pronounced change highlighting the interface between the dense coacervate phase and the dilute phase. The interface is indicated by a vertical grey dashed line and is defined as the position where the electrostatic potential  $\psi(x)$  takes half the value between dense coacervate and dilute phase. The concentration profiles are not symmetric and deviate from the classical interface profile obtained for a symmetric binary Ginzburg-Landau free energy [33, 34]. The reason is that the mixture is ternary and molecular volumes of the charged components are different. For decreasing relative gradient cost ratio  $\kappa_p$  (the ratio  $\kappa_p/\kappa_-$  is varied by only varying  $\kappa_p$  while keeping  $\kappa_-$  fixed), the concentration profiles become steeper around the interface as the energy cost associated with keeping gradients goes down. We also note that although the relative gradient cost ratio  $\kappa_p/\kappa_-$  is varied by only varying  $\kappa_p$  while keeping  $\kappa_-$  fixed, both  $n_p$  and  $n_-$  show the same behavior with changing  $\kappa_p$ .

A key finding of our work is that charges can separate within the interfacial domain which is evident in the spatially varying charge density  $\rho(x)$  (Fig. 2(b)). While the mixture is charge-neutral ( $\rho(x) \simeq 0$ ) deeply in the dense coacervate and dilute phase, we find multiple domains with a positive or negative charge density. The gradient cost  $\kappa_p$  essentially determines the shape and the amplitudes of the charge density. For the considered parameters, there is a pronounced negatively charged domain at  $x > 0$ , and a pronounced positively charged domain at  $x < 0$ .

This separation of charge leads to a complex behavior of the electrostatic potential  $\psi(x)$  within the interfacial domain (Fig. 2(c)). The negatively charged domain at  $x > 0$  gives rise to a potential well relative to the reference potential in the dilute phase that is chosen to be zero. On the contrary, the positively charged domain at  $x < 0$  causes a barrier of the electrostatic potential relaxing toward the Donnan potential  $\psi_D$  inside the dense phase [35, 36]. The electrostatic potential well and barrier implies that a positive test charge would get attracted into the well and repelled by the potential barrier. The existence and strength of both characteristics is set by the cost ratio  $\kappa_p$ . For large values, the well and the potential barrier vanishes. The reason is that the charge density in the interface approaches concomitantly to zero (Fig. 2(b)) since the free energy penalty for gradients becomes too large for increasing  $\kappa_p$ .

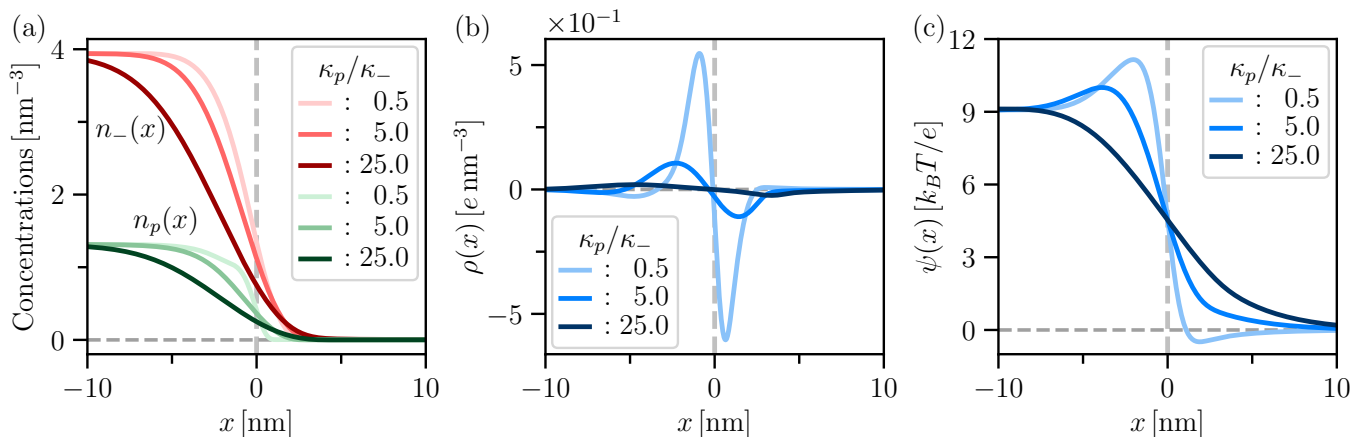


FIG. 2. **Interfacial charge separation of simple coacervates without salt.** (a) Concentration profiles of charged components  $n_i(x)$ , where ( $p$ ) and ( $-$ ) indicates the macromolecule and counterion, respectively. For increasing  $\kappa_p$ , the profiles steepen around the interface indicated by a vertical dashed line. (b) The charge density  $\rho(x) = e(q_p n_p(x) + q_- n_-(x))$  indicates separation of charged components in the interfacial domain for small enough  $\kappa_p$ . Only in this case, the free energy penalty is low enough such that interactions of the charged components with the solvent can give rise to a non-zero charge density. (c) The electrostatic potential  $\psi(x)$  has a complex shape within the interfacial domain. There is a well in the negatively charged domain and a barrier in the positively charged domain. The potential is set to zero far in the dilute phase. The interface position is defined where the electrostatic potential is half the value deeply inside the dense coacervate phase.

## 2. Impact of salt on simple coacervates

Now we consider a system that, in addition to the positively charged macromolecules and its counterions, contains salt. For simplicity we consider a monovalent salt and do not make any distinction between the counterions and the anions released by the salt. The resulting quaternary mixture thus contains macromolecules ( $p$ ), cations ( $+$ ), anions ( $-$ ), and solvent ( $s$ ) molecules. For results discussed in this section, we choose the molecular volumes and the interaction parameters as follows:  $\nu_p/\nu_s = \nu_p/\nu_+ = \nu_p/\nu_- = 30$ , and  $\chi_{ps} = 1.9 \text{ nm}^{-3}$ ,  $\chi_{p+} = 1.8 \text{ nm}^{-3}$ ,  $\chi_{p-} = -1.8 \text{ nm}^{-3}$ ,  $\chi_{+-} = \chi_{+s} = \chi_{-s} = -0.09 \text{ nm}^{-3}$ . We also set  $\kappa_+ = \kappa_- = \kappa$  and unless stated otherwise, use  $\kappa = 15 k_B T \text{ nm}^5$ .

The concentration profiles of charged components  $n_i(x)$  in simple coacervates with salt ( $i = p, +, -$ ) show a complex behavior close to the interface (Fig. 3(a)), where the interface is indicated by a vertical dashed line. The macromolecule concentration  $n_p(x)$  decreases monotonically together with the oppositely charged counter-ion ( $-$ ) when passing from the dense coacervate phase toward the dilute phase. This coupled behavior is a result of the attractive electrostatic interactions. Interestingly, the positively charged co-ions ( $+$ ) vary non-monotonically, i.e., ( $+$ )-ions accumulate right outside the coacervate phase. This accumulation is a result of a macromolecule-poor layer right outside the coacervate and is formed by the attractive electrostatic interactions between oppositely charged ions. This variation vanishes with increasing cost ratio  $\kappa_p$  as the profile of macromolecules at the interface flattens and thereby contributes to neutralizing the interfacial domain.

The charge density  $\rho(x)$  and the electrostatic potential  $\psi(x)$  have a similar qualitative behavior as compared to the case without salt. Multiple charge layers of alternating charge develop within the interfacial region (Fig. 3(b)) and the electrostatic potential can vary non-monotonically with potential wells and barriers (Fig. 3(c)). These profile characteristics vanish for increasing  $\kappa_p$  as it quantifies the free energy penalty for profile heterogeneities. However, the presence of salt quantitatively makes charge separation more pronounced, i.e., it is observed for even higher values of  $\kappa_p$ .

The well and barrier of the electrostatic potential is determined by the salt concentration  $c_{\text{salt}}$ . To quantify this impact, we introduce the interfacial potential  $\psi_{\text{int}}$  as the potential difference between the barrier and the well minimum and contrast it with the Donnan potential  $\psi_D$  (Fig. 4(a)). We also propose a definition for the interface width of the coacervate  $\Delta$  as the distance between the position of potential well and barrier. We find that the Donnan potential  $\psi_D$  and the interfacial potential  $\psi_{\text{int}}$  decrease with the salt concentration  $c_{\text{salt}}$  (Fig. 4(b)). This decrease is due to screening as more salt reduces the electrostatic interactions of the phase-separated macromolecules. For large salt concentrations, this decrease weakens and crosses over to a logarithmic decay for both  $\psi_D$  and  $\psi_{\text{int}}$ , each decaying with a characteristic salt concentration (Fig. 7 in Appendix A). The decrease of  $\psi_D$  and  $\psi_{\text{int}}$  with salt is however extremely insensitive to the average macromolecule concentration  $\bar{n}_p$ . The latter predominantly sets the size of the coacervate without altering the composition significantly. For sufficiently large values of the gradient cost  $\kappa_p$  the potential profiles become monotonically varying leading to a vanishing difference

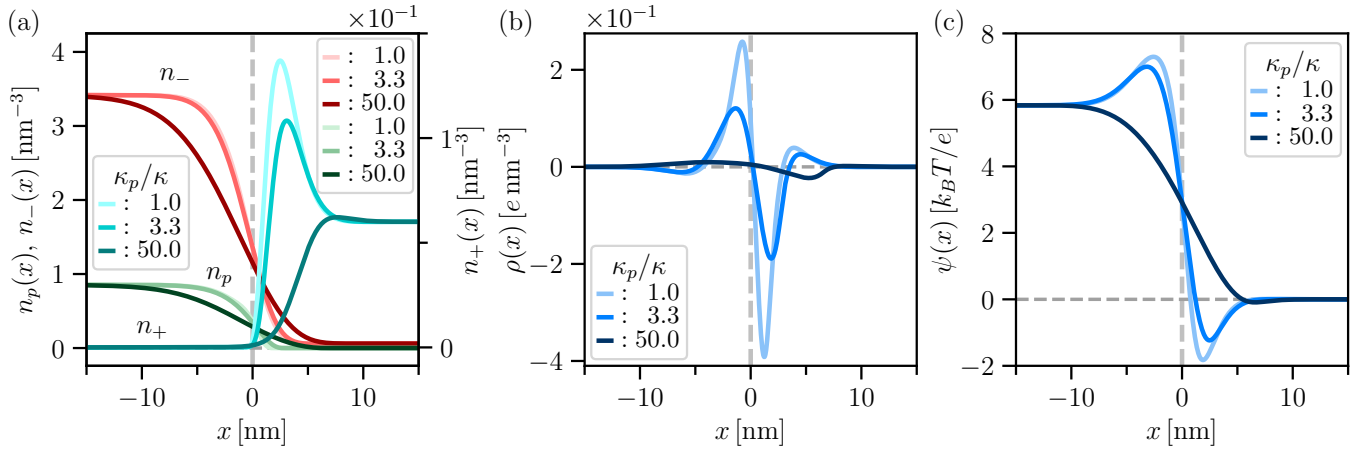


FIG. 3. **Interfacial charge separation of simple coacervates with salt.** (a) In contrast to the case without salt (Fig. 2), the concentration profiles of charged components  $n_i(x)$  ( $i = p, -, +$ ) can vary in a non-monotonic fashion within the interfacial domain; the interface is indicated by the vertical dashed line. The dense coacervate phase is enriched in positively charged macromolecules together with its neutralizing counter-ions ( $-$ ), while the positively charged co-ions ( $+$ ) accumulate adjacent to the interface toward the dilute phase. This accumulation enhances for decreasing  $\kappa_p$ . (b) The charge density  $\rho(x) = e(q_p n_p(x) + q_- n_-(x) + q_+ n_+(x))$  shows, as in the case without salt, that charges separate in the interfacial domain and that charge separation is more pronounced for smaller  $\kappa_p$ . (c) The associated electrostatic potential  $\psi(x)$  exhibits potential wells and barriers that are even more pronounced compared to the case without salt. The plots correspond to a system with salt concentration  $c_{\text{salt}} = 100$  mM, a macromolecular charge  $q_p = +4$  and average concentration  $\bar{n}_p = 0.1$  mM, and ion charges  $q_{\pm} = \pm 1$ .

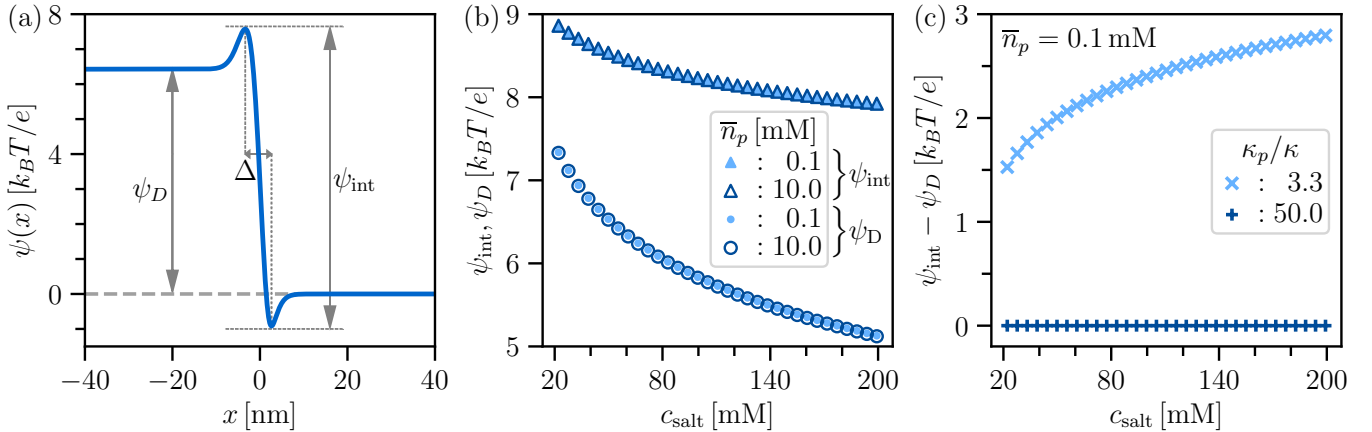


FIG. 4. **Impact of salt on the electrostatic potential of simple coacervates.** (a) Illustration of the Donnan potential  $\psi_D$ , the interfacial potential  $\psi_{\text{int}}$  and the interfacial width  $\Delta$  for a representative electrostatic potential profile  $\psi(x)$  obtained for simple coacervates. (b) The Donnan potential  $\psi_D$  and the interfacial potential  $\psi_{\text{int}}$  decrease with salt concentration  $c_{\text{salt}}$  since salt screens the electrostatic interactions. The average macromolecule concentration  $\bar{n}_p$  in the system hardly affects  $\psi_D$  or  $\psi_{\text{int}}$  as it mainly alters the size of the dense coacervate phase. (c) For a large value of  $\kappa_p = 50$ , the potential profile varies monotonically and  $\psi_{\text{int}} - \psi_D$  vanishes. Thus, there are no additional potential barriers and wells. For small enough values of  $\kappa_p$ , the difference between Donnan and interfacial potential  $\psi_{\text{int}}$  and  $\psi_D$  is non-zero and increases with salt concentration  $c_{\text{salt}}$ . The reason is that salt reduces the electrostatic potential by screening, which is more pronounced in the bulk phases due to the ions' gradient costs. We fixed average macromolecule concentration  $\bar{n}_p = 0.1$  mM. For all the plots here, macromolecule charge  $q_p = 4$ , co/counter-ion charges  $q_{\pm} = \pm 1$  are used.

( $\psi_{\text{int}} - \psi_D$ ) (Fig. 4(c)); see Fig. 3(c) for the corresponding electrostatic potential profiles. However, lowering the  $\kappa_p$ -values leads to barriers and wells of the electrostatic potential and thereby a non-zero differences ( $\psi_{\text{int}} - \psi_D$ ). Interestingly, though both the Donnan potential  $\psi_D$  and

the interfacial potential  $\psi_{\text{int}}$  decrease with increasing salt, their difference increases (Fig. 4(c)). This trend indicates that the electrostatic potential differences between the dense coacervate phase and the dilute phase is more affected by salt screening than the interfacial potential.

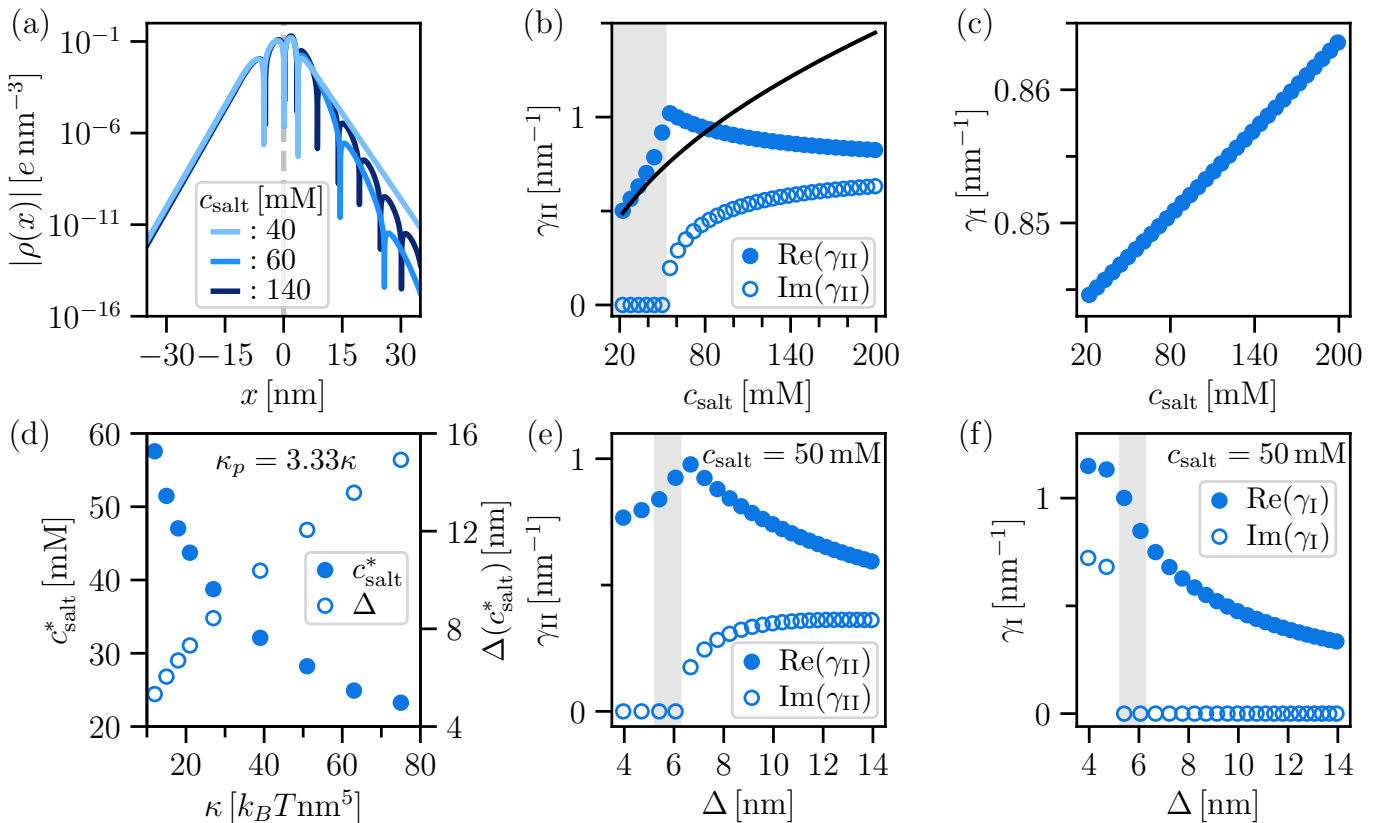


FIG. 5. **Layers of alternating charge density in the dense coacervate and dilute phase.** (a) Logarithmic representation of the absolute value of the charge density  $|\rho(x)|$  around the interfacial domain indicates layers of alternating charge density. The amplitude of charge density  $|\rho(x)|$  within layers decay approximately exponentially with characteristic length scales  $\text{Re}(\gamma_{I/II})^{-1}$  that are phase-dependent. The width of charged layers that can be characterized by  $\text{Im}(\gamma_{I/II})^{-1}$ , decreases with increasing salt concentration  $c_{\text{salt}}$ . (b) In the dilute phase,  $\text{Re}(\gamma_{II})$  shows a non-monotonic behavior. A non-zero  $\text{Im}(\gamma_{II})$  indicates the existence of layers of alternating charge. Layers only occur for salt concentrations above the threshold  $c_{\text{salt}}^*$ . For  $c_{\text{salt}} > c_{\text{salt}}^*$ ,  $\text{Re}(\gamma_{I/II})$  decreases with salt indicating a deviation from classical Debye-Hückel theory. Here we used  $\kappa = 15 k_B T \text{nm}^{-5}$ . (c) In the coacervate phase,  $\text{Re}(\gamma_I)$  changes only weakly with salt and there are no layers deeply in the coacervate phase ( $\text{Im}(\gamma_I) = 0$ ). (d) The threshold salt concentration  $c_{\text{salt}}^*$  decreases with increasing interfacial width  $\Delta$ , where  $\Delta$  can be changed by the gradient cost  $\kappa$ . (e,f) Increasing the interfacial width  $\Delta$  makes the system crossing from a situation where alternating charged layers solely exist inside the coacervate, over a regime without any layers, to a regime with layers present exclusively in the dilute phase. For all panels, we use  $\bar{n}_p = 0.1 \text{mM}$ ,  $\kappa_+ = \kappa_- = \kappa$ ,  $\kappa_p = 3.33\kappa$ . In panels (e) and (f), the interfacial width  $\Delta$  is varied by varying  $\kappa$  in the range  $(6 - 75) k_B T \text{nm}^{-5}$ . Further parameters are the same as in Fig. 4. The grey shaded regions in panels (b), (e), (f) indicate situations where imaginary part of the decay constant is zero in both phases.

This asymmetry between bulk phases and interfacial domains arise from the additional gradient cost compared to the bulk phases for the counter-ions to accumulate in the interfacial domains.

The salt concentration determines the amount and the size of the layers within the interfacial domain. A logarithmic representation of the absolute value of the charge density  $|\rho(x)|$  reveals that multiple layers of alternating charge extend from the interfacial domain towards the dense and dilute phase, respectively (Fig. 5(a)). Increasing the salt concentration increases the number of such layers and decreases layer width. To quantify the layering with salt, we calculated the real and imaginary part of  $\gamma_{I/II}$  deeply in the dense coacervate and dilute phase by linearizing the profile of each component  $i$  around phase equilibrium  $n_i^0$  by writing  $n_i(x) = n_i^0 + c_i \exp(\gamma x)$ ; for

details see Appendix B. We find that amplitudes of charge density  $|\rho(x)|$  in the layers decay approximately exponentially with a characteristic length scale  $\text{Re}(\gamma_{I/II})^{-1}$ ; an effect reminiscent of classical electrostatic screening as described by the Debye-Hückel theory [37], where  $\text{Re}(\gamma)^{-1}$  would correspond to the Debye screening length. For our simple coacervate in the presence of salt,  $\text{Re}(\gamma_{II})$  shows a non-monotonic behavior with salt (Fig. 5(b)). For low salt, it increases with increasing salt concentration which is consistent with Debye-Hückel theory. However, when passing a threshold salt concentration  $c_{\text{salt}}^*$ , this behavior qualitatively changes as  $\text{Re}(\gamma_{II})$  decreases with increasing salt concentration. The threshold  $c_{\text{salt}}^*$  coincides with the appearance of a non-zero imaginary part  $\text{Im}(\gamma_{II})$  which indicates the existence of layers of alternating charge also far away from the coacervate interface. In other

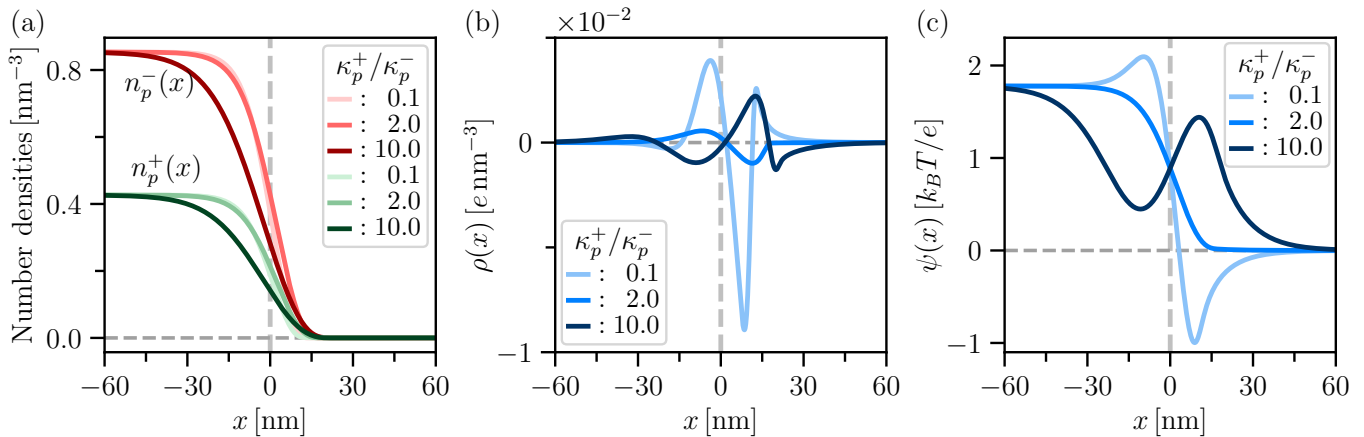


FIG. 6. **Interfacial charge separation of complex coacervates.** (a) Monotonic decrease of concentration profiles of the macromolecules  $n_p^\pm(x)$  within the interfacial domain. (b) The charge density  $\rho(x) = e(q_p^+ n_p^+(x) + q_p^- n_p^-(x))$  shows complex spatial variation inside the interfacial domain indicating that charge separation can also occur for complex coacervation. By altering the relative gradient cost  $\kappa_p^+$  of the oppositely charged macromolecules, the charged layers can swap their sign. (c) This swapping is evident in the corresponding behavior of the electrostatic potential profile  $\psi(x)$  when changing  $\kappa_p^+$ . The ordering of potential barriers and wells swaps. The vertical dashed line in each plot marks the location of the interface. As parameters, we use  $q_p^+ = 4$ ,  $q_p^- = -2$  together with other parameters mentioned in Sect. III B.

words, the bulk phases can be layered reminiscent of block co-polymers undergoing microphase separation [38–40]. However, the amplitudes of such layers are exponentially damped implying that the manifestation of layering gets negligible deeply in the respective phases. Moreover, for the considered parameters in Fig. 5(a-c), we have found that layers not necessarily exist in both coexisting phases; here we show an example where the dilute phase is layered while the dense coacervate phase is not (Fig. 5(b,c)). Though layers have been reported in theories at charged solid interfaces [41, 42], layering around liquid interface is distinct as the additional interfacial width is coupled to the spatial variations extending towards both bulk phases.

The interfacial width  $\Delta$  of the coacervate strongly affects the threshold  $c_{\text{salt}}^*$  of charge layering (Fig. 5(d)). The interfacial width can be changed by increasing the parameter characterizing the gradient cost  $\kappa$ , where we chose  $\kappa_+ = \kappa_- = \kappa$ . Thus, for larger  $\Delta$ , the threshold for layering,  $c_{\text{salt}}^*$ , decreases.

The interfacial width  $\Delta$  also controls whether layers of alternating charge occur in the dilute or in the coacervate phase (Fig. 5(e,f)). For low interfacial width  $\Delta$  the dense coacervate phase (Fig. 5(f)) exhibits layers, while the dilute phase does not. Increasing  $\Delta$  leads to a domain where none of the phases have layers (gray shaded domain in Figs. 5(b,e,f)). For even larger value of the interfacial width  $\Delta$ , the coacervate is not layered while the dilute phase has layers of alternating charge (Fig. 5(e)).

## B. Complex coacervates

Here we discuss a minimal model for complex coacervation and scrutinize our key finding of charge separation

at the interface. In contrast to a simple coacervate, complex coacervation is driven by the attractive electrostatic interaction between (at least) two oppositely charged macromolecules. As a result, both macromolecule types are enriched inside the coacervate phase compared to the coexisting dilute phase. Our minimal model for a complex coacervate accounts for two oppositely charged macromolecules ( $p^+$  and  $p^-$ ) suspended in a solvent ( $s$ ). For the following studies, we consider macromolecule-solvent molecular volume ratios  $\nu_p^+/\nu_s = \nu_p^-/\nu_s = 20$  and Flory-Huggins parameters  $\chi_{p^+s} = 1.0 \text{ nm}^{-3}$ ,  $\chi_{p^-s} = 0.6 \text{ nm}^{-3}$ , and  $\chi_{p^+p^-} = -1.0 \text{ nm}^{-3}$ .

The concentration profiles of the macromolecules  $n_p^\pm(x)$  vary monotonously (Fig. 6(a)). We could not find any additional concentration layers as observed for simple coacervates with salt. However, the charge density can exhibit spatial variation in the interfacial domain indicating that charges can separate also for complex coacervates (Fig. 6(b)). We have varied the relative gradient cost of the positively to the negatively charged macromolecule,  $\kappa_p^+/\kappa_p^-$  by varying  $\kappa_p^+$ . We find that  $\kappa_p^+$  can flip the charge of the layers when passing through the interfacial domain. For  $\kappa_p^+ \ll \kappa_p^-$ , the gradients of the concentration field  $n_p^+$  can be steeper compared to that of  $n_p^-$ . Therefore, right inside the coacervate one has  $n_p^+ > n_p^-$  leading to a positively charged layer. In the other limit, i.e., for  $\kappa_p^+ \gg \kappa_p^-$ , the gradients of the concentration field  $n_p^+$  becomes less steeper compared to that of  $n_p^-$ . Therefore, one obtains the swapped case with  $n_p^- > n_p^+$  and a negatively charged layer right inside the coacervate. This swapping becomes also evident in the behavior of the electrostatic potential  $\psi(x)$  as a function of the relative gradient cost  $\kappa_p^+$ . While for small  $\kappa_p^+ \ll \kappa_p^-$ , the coacervate phase comprises a

potential barrier and the dilute phase a potential well, this swaps for large  $\kappa_p^+ \gg \kappa_p^-$ .

#### IV. CONCLUSIONS

In summary, we present a theoretical framework to study profiles of concentrations and electrostatic potential at interfaces of phase-separated solution containing charged components. We apply this framework to simple and complex coacervates. Our approach extends the Poisson-Boltzmann theory that describes the spatial distributions of ions adjacent to charged, solid surfaces or charged colloidal particles. In these systems counter-ions typically follow a Boltzmann distribution and screen the surface charge. Our extension accounts for the interactions among all charged components taking into account phase coexistence. Our work therefore provides a framework for coacervation at salt concentrations where the Poisson-Boltzmann theory fails [19]. Most importantly, in phase-separated systems, interfaces are associated with free energy costs for gradients of charged and uncharged components. These contributions are lacking in the classical Poisson-Boltzmann theory.

The key finding of our theory is that, in simple and complex coacervates, interfaces between coexisting phases give rise to a charge separation in the interfacial domain. Beyond a threshold salt concentration, multiple layers of alternating charges can occur around the interface which extend into the bulk phases. However, the amplitude of the charge contained in each layer decreases exponentially for increasing distance from the interface. We show that salt regulates the number and the width of such layers of alternating charges. Similar layering has previously been reported in non-phase separated systems for large salt concentrations resulting from correlations beyond mean-field as well as within mean-field description [41–46]. Our studies show that layering can occur at mean-field level with moderate salt concentrations due to phase separation where the interfacial width control the layer patterns.

Charged layers localized around the interface can affect interfacial transport. An interesting case is the stochastic trajectory of single charged probe molecules diffusing across the interface. This molecule will encounter the electric potential profile with barriers and traps which affects the transport kinetics. The resulting charge-specific reflection or trapping of the probe at the interface suggests charge-dependent transport properties at the interface. In the context of biomolecular condensates forming via phase separation in cells [1], this phenomenon could be used by cells to regulate molecular transport; a property usually associated with membranes [47, 48].

Our finding of complex-shaped charged layers at the coacervate interfaces implies that a coacervate is not a colloid with a surface charge surrounded by a (dilute) layer of screening counter-ions. Counter-ions at coacervate interfaces are, in general, non-dilute and participate in the phase separation equally as the macromolecules.

In other words, the surface charge is not solely a property of the coacervate, as is typically the case for colloids. For coacervates, the surface charge depends on the interactions and concentrations of all charged components in the system. Thus, changes in salt or gradient costs alter the coacervate’s surface charge and the screening counter-ion distribution. This complexity poses an exciting challenge in calculating the electrophoretic mobility when coacervates are subject to external electric fields [24, 26].

Our theoretical framework paves the way to investigating even more complex phase separation phenomena in non-dilute mixtures composed of charged components. It remains elusive why coacervates hardly undergo coarsening by Ostwald ripening [17, 49, 50], and why coacervates can repel each other or stick without fusing [51]. Moreover, the surface charge of coacervates could also be regulated by pH [29, 30], and coacervates can also act as chemical reactors [52–54]. Recently, coacervates maintained away from equilibrium were shown to deform to complex shapes, including the formation of liquid shells [55, 56].

#### ACKNOWLEDGMENTS

We thank L. Hubatsch for fruitful discussion on the topics of interfacial transport and P. M. McCall for general discussions on electrostatics of protein droplets. F. Jülicher acknowledges funding by the Volkswagen Foundation. C. Weber acknowledges the European Research Council (ERC) under the European Union’s Horizon 2020 research and innovation programme (“Fuelled Life” with Grant agreement No. 949021) for financial support.

#### Appendix A: $\psi_D$ and $\psi_{\text{int}}$ as function of salt concentration

In Fig. 4 of the main text, we have shown the variations of the Donnan potential  $\psi_D$  and the interfacial potential  $\psi_{\text{int}}$  as functions of the salt concentration  $c_{\text{salt}}$  using linear scales. In order to gain further insight into the actual variation, here we plot them for an even larger salt concentration range using semi-log scale. As the plots suggest, both  $\psi_D$  and  $\psi_{\text{int}}$  varies logarithmically with  $c_{\text{salt}}$  but with different rates.

#### Appendix B: Expansion around phase equilibrium for a ternary system

Let us consider a ternary system consisting of a positively charged species (+), a negatively charged species (−) and a solvent ( $s$ ). Conservation of volume fractions implies that all of the three volume fractions are not independent of each other. As always, we consider the one for the solvent to be the dependent one which is given by  $(1 - \nu_+ n_+ - \nu_- n_-)$ . The other two volume fractions or equivalently, the corresponding concentration profiles



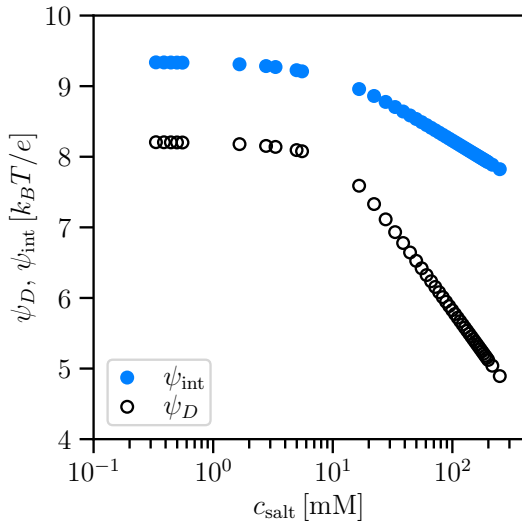


FIG. 7. Variation of both the Donnan potential  $\psi_D$  and the interfacial potential  $\psi_{\text{int}}$  (defined in Fig. 4(a)) as functions of the salt concentration  $c_{\text{salt}}$  showing that  $\psi_D$  and  $\psi_{\text{int}}$  varies logarithmically for large  $c_{\text{salt}}$  but with different rates.

(as we consider constant molecular volumes  $\nu_{\pm}$ ) together with the electrostatic potential everywhere in the system can be obtained by solving the following equations:

$$\nabla^2 \psi = -\frac{\rho}{\varepsilon}, \quad (\text{B1})$$

$$\mu_{\pm}^{\text{el}} = \text{constant}. \quad (\text{B2})$$

Away from the interface, all the quantities decay exponentially as

$$n_+ = n_+^0 + c_+ \exp(\gamma x), \quad (\text{B3})$$

$$n_- = n_-^0 + c_- \exp(\gamma x), \quad (\text{B4})$$

$$\psi = \psi^0 + c_{\psi} \exp(\gamma x), \quad (\text{B5})$$

to their respective bulk values, i.e., to  $n_+^0$ ,  $n_-^0$ , and  $\psi^0$  with a decay constant  $\gamma$ . As there are three equations to solve for four variables, one can obtain only the ratios  $c_p = c_+/c_{\psi}$  and  $c_m = c_-/c_{\psi}$ . Inserting the exponential profiles back into the Poisson equation (B1), one obtains the condition

$$\gamma^2 = -\frac{q_+ c_p + q_- c_m}{\varepsilon}. \quad (\text{B6})$$

Next, the exponential profiles are inserted into the equal exchange electrochemical potential conditions:  $\mu_{\pm}^{\text{el}}(\text{I}) = \mu_{\pm}^{\text{el}}(\text{II})$ , where I and II refers to the dense and the dilute phases, respectively (see Fig. 1). The log terms are expanded up to linear order with respect to small deviations

from the bulk densities in the following way:

$$\begin{aligned} \log(\nu_i n_i) &= \log(\nu_i n_i^0 + \nu_i c_i \exp(\gamma x)) \\ &= \log\left[\nu_i n_i^0 \left(1 + \frac{c_i}{n_i^0} \exp(\gamma x)\right)\right] \\ &= \log(\nu_i n_i^0) + \log\left(1 + \frac{c_i}{n_i^0} \exp(\gamma x)\right) \\ &= \log(\nu_i n_i^0) + \frac{c_i}{n_i^0} \exp(\gamma x) + \dots, \end{aligned} \quad (\text{B7})$$

and

$$\begin{aligned} \log(1 - \nu_+ n_+ - \nu_- n_-) &= \log\left[1 - \nu_+ n_+^0 - \nu_- n_-^0 - (\nu_+ c_+ - \nu_- c_-) \exp(\gamma x)\right] \\ &= \log\left[\phi_s^0 \left(1 - \frac{\nu_+ c_+}{\phi_s^0} \exp(\gamma x) - \frac{\nu_- c_-}{\phi_s^0} \exp(\gamma x)\right)\right] \\ &= \log(\phi_s^0) + \log\left(1 - \frac{\nu_+ c_+}{\phi_s^0} \exp(\gamma x) - \frac{\nu_- c_-}{\phi_s^0} \exp(\gamma x)\right) \\ &= \log(\phi_s^0) - \frac{\nu_+ c_+}{\phi_s^0} \exp(\gamma x) - \frac{\nu_- c_-}{\phi_s^0} \exp(\gamma x) + \dots, \end{aligned} \quad (\text{B8})$$

where  $\phi_s^0 = 1 - \nu_+ n_+^0 - \nu_- n_-^0$ . Using these expressions in the constant exchange electrochemical potential conditions and equating the coefficients of  $\exp(\gamma x)$  to zero, one obtains:

$$\begin{aligned} \kappa_+ \gamma^2 c_p &= q_+ + \frac{c_p}{n_+^0} + \frac{\nu_+}{\nu_s} \left(\frac{\nu_+ c_p}{\phi_s^0} + \frac{\nu_- c_m}{\phi_s^0}\right) + \chi_{+-} c_m \\ &\quad - \chi_{+s} \left(2 \frac{\nu_+}{\nu_s} c_p + \frac{\nu_-}{\nu_s} c_m\right) - \chi_{-s} \frac{\nu_+}{\nu_s} c_m \end{aligned} \quad (\text{B9})$$

and

$$\begin{aligned} \kappa_- \gamma^2 c_m &= q_- + \frac{c_m}{n_-^0} + \frac{\nu_-}{\nu_s} \left(\frac{\nu_+ c_p}{\phi_s^0} + \frac{\nu_- c_m}{\phi_s^0}\right) + \chi_{+-} c_p \\ &\quad - \chi_{-s} \left(2 \frac{\nu_-}{\nu_s} c_m + \frac{\nu_+}{\nu_s} c_p\right) - \chi_{+s} \frac{\nu_-}{\nu_s} c_p \end{aligned} \quad (\text{B10})$$

Finally, after doing some algebraic manipulation, Eqs. (B6), (B9), and (B10) lead to the following polynomial equation satisfied by the decay constant  $\gamma$ :

$$\begin{aligned} \varepsilon \kappa_+ \kappa_- \gamma^6 - \varepsilon (a \kappa_- + d \kappa_+) \gamma^4 \\ + (\varepsilon a d - \varepsilon b^2 + q_+^2 \kappa_- + q_-^2 \kappa_+) \gamma^2 \\ + (2b q_+ q_- - q_+^2 d - q_-^2 a) = 0, \end{aligned} \quad (\text{B11})$$

where

$$a = \frac{1}{n_+^0} + \frac{\nu_+^2}{\nu_s \phi_s^0} - 2 \chi_{+s} \frac{\nu_+}{\nu_s}, \quad (\text{B12})$$

$$b = \frac{\nu_+ \nu_-}{\nu_s \phi_s^0} + \chi_{+-} - \chi_{+s} \frac{\nu_-}{\nu_s} - \chi_{-s} \frac{\nu_+}{\nu_s}, \quad (\text{B13})$$

$$d = \frac{1}{n_-^0} + \frac{\nu_-^2}{\nu_s \phi_s^0} - 2 \chi_{-s} \frac{\nu_-}{\nu_s}. \quad (\text{B14})$$

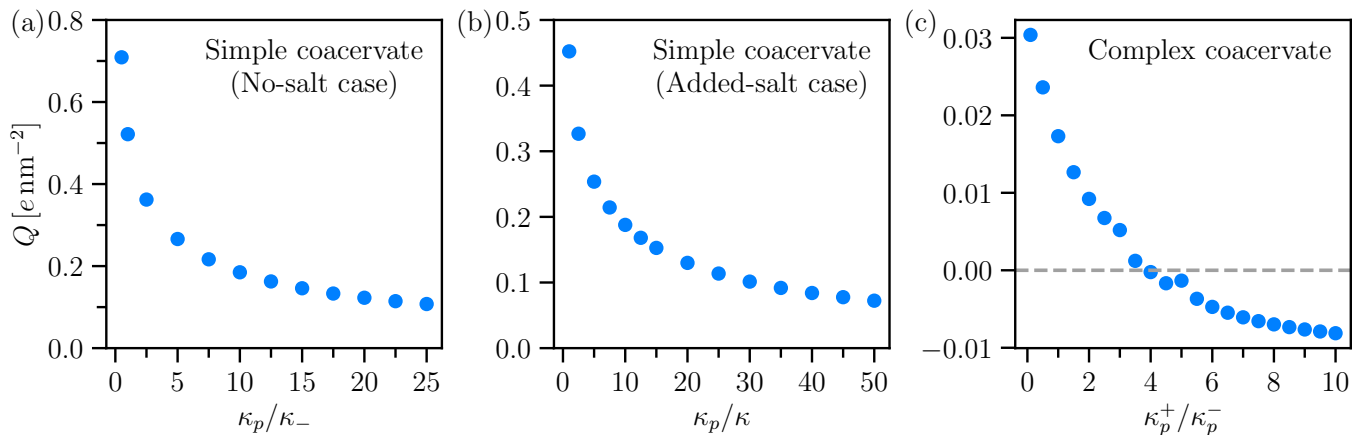


FIG. 8. Variation of both the total charge contained within the coacervate phase as function of the relative gradient cost parameters for (a) simple coacervates without salt, (b) simple coacervates with salt as well as for (c) complex coacervates. Whereas for the simple coacervates the total charge of the coacervate remains of same sign with changing relative gradient cost, for complex coacervates it can even change sign.

This can be solved to find the six roots and typically, the smallest one survives in the large asymptotic limit (i.e., for large  $|x|$ -values in either phase away from the interface at  $x = 0$ ). A similar calculation can be done for a quaternary system which leads to a polynomial equation of higher degree.

### Appendix C: Total charge $Q$ inside the coacervate phase

In Fig. 8, we plot the total charge

$$Q = \int_{-\infty}^0 dx \rho(x) \quad (\text{C1})$$

contained inside the coacervate phase for three different cases (simple coacervates with or without salt and complex coacervates). As one can see, in all three cases, the total charge  $Q$  decreases with increasing gradient cost ratios. In addition, it can even flip sign for complex coacervates. The kinks in the curve corresponding to complex coacervates (Fig. 8(c)) correspond to changes in the shape of the electrostatic potential profiles as depicted in Fig. 6(c). We note that the position of the interface, i.e., the location  $x = 0$  is defined based on the electrostatic potential profiles. In cases the potential profile encounters the value  $\psi_D/2$  more than once, we choose the middle one to be the location of the interface.

- 
- [1] A. A. Hyman, C. A. Weber, and F. Jülicher, Liquid-liquid phase separation in biology, *Annu. Rev. Cell Dev. Biol.* **30**, 39 (2014).
  - [2] Y. Shin and C. P. Brangwynne, Liquid phase condensation in cell physiology and disease, *Science* **357**, eaaf4382 (2017).
  - [3] H. L. Booij and H. G. Bungenberg de Jong, *Biocolloids and their Interactions*, 1st ed. (Springer Vienna, 1956).
  - [4] A. I. Oparin, *The Origin of Life on the Earth*, 3rd ed. (Academic Press Inc., 1957).
  - [5] J. W. Szostak, D. P. Bartel, and P. L. Luisi, Synthesizing life, *Nature* **409**, 387 (2001).
  - [6] G. Bartolucci, A. C. Serrão, P. Schwintek, A. Kühnlein, Y. Rana, P. Janto, D. Hofer, C. B. Mast, D. Braun, and C. A. Weber, Selection of prebiotic oligonucleotides by cyclic phase separation (2022), [arXiv:2209.10672](https://arxiv.org/abs/2209.10672) [physics.chem-ph].
  - [7] C. P. Brangwynne, C. R. Eckmann, D. S. Courson, A. Rybarska, C. Hoege, J. Gharakhani, F. Jülicher, and A. A. Hyman, Germline p granules are liquid droplets that localize by controlled dissolution/condensation, *Science* **324**, 1729 (2009).
  - [8] J. Guillén-Boixet, A. Kopach, A. S. Holehouse, S. Wittmann, M. Jahnel, R. Schließler, K. Kim, I. R. Trussina, J. Wang, D. Mateju, I. Poser, S. Maharana, M. Ruer-Gruß, D. Richter, X. Zhang, Y.-T. Chang, J. Guck, A. Honigmann, J. Mahamid, A. A. Hyman, R. V. Pappu, S. Alberti, and T. M. Franzmann, RNA-induced conformational switching and clustering of g3bp drive stress granule assembly by condensation, *Cell* **181**, 346 (2020).
  - [9] A. W. Fritsch, A. F. Diaz-Delgadillo, O. Adame-Arana, C. Hoege, M. Mittasch, M. Kreysing, M. Leaver, A. A. Hyman, F. Jülicher, and C. A. Weber, Local thermodynamics govern formation and dissolution of *Caenorhabditis*

- elegans P granule condensates, *Proc. Natl. Acad. Sci.* **118**, e2102772118 (2021).
- [10] S. F. Banani, H. O. Lee, A. A. Hyman, and M. K. Rosen, Biomolecular condensates: organizers of cellular biochemistry, *Nat. Rev. Mol. Cell Biol.* **18**, 285–298 (2017).
- [11] T. M. Franzmann and S. Alberti, Protein phase separation as a stress survival strategy, *Cold Spring Harbor Perspect. Biol.* **11**, a034058 (2019).
- [12] T. M. Franzmann, M. Jahnel, A. Pozniakovskiy, J. Mahamid, A. S. Holehouse, E. Nüske, D. Richter, W. Baumeister, S. W. Grill, R. V. Pappu, A. A. Hyman, and S. Alberti, Phase separation of a yeast prion protein promotes cellular fitness, *Science* **359**, eaao5654 (2018).
- [13] T. Lu and E. Spruijt, Multiphase complex coacervate droplets, *J. Am. Chem. Soc.* **142**, 2905 (2020).
- [14] L. M. Jawerth, M. Ijavi, M. Ruer, S. Saha, M. Jahnel, A. A. Hyman, F. Jülicher, and E. Fischer-Friedrich, Salt-dependent rheology and surface tension of protein condensates using optical traps, *Phys. Rev. Lett.* **121**, 258101 (2018).
- [15] L. Hubatsch, L. M. Jawerth, C. Love, J. Bauermann, T. D. Tang, S. Bo, A. A. Hyman, and C. A. Weber, Quantitative theory for the diffusive dynamics of liquid condensates, *Elife* **10**, e68620 (2021).
- [16] P. M. McCall, K. Kim, A. W. Fritsch, J. Iglesias-Artola, L. Jawerth, J. Wang, M. Ruer, J. Peychl, A. Poznyakovskiy, J. Guck, S. Alberti, A. A. Hyman, and J. Brugués, Quantitative phase microscopy enables precise and efficient determination of biomolecular condensate composition, *bioRxiv* <https://doi.org/10.1101/2020.10.25.352823> (2023).
- [17] M. Abbas, W. P. Lipiński, J. Wang, and E. Spruijt, Peptide-based coacervates as biomimetic protocells, *Chem. Soc. Rev.* **50**, 3690 (2021).
- [18] J. T. G. Overbeek and M. J. Voorn, Phase separation in polyelectrolyte solutions. theory of complex coacervation, *J. Cell. Comp. Physiol.* **49**, 7 (1957).
- [19] M. Boström, D. R. M. Williams, and B. W. Ninham, Specific ion effects: Why DLVO theory fails for biology and colloid systems, *Phys. Rev. Lett.* **87**, 168103 (2001).
- [20] R. M. Adar, T. Markovich, and D. Andelman, Bjerrum pairs in ionic solutions: A Poisson-Boltzmann approach, *J. Chem. Phys.* **146**, 194904 (2017).
- [21] D. S. Dean, J. Dobnikar, A. Naji, and R. Podgornik, eds., *Electrostatics of Soft and Disordered Matter*, 1st ed. (CRC Press, Taylor & Francis Group, Boca Raton, FL, 2014).
- [22] T. Markovich, D. Andelman, and R. Podgornik, Charged membranes: Poisson–Boltzmann theory, the DLVO paradigm, and beyond, in *Handbook of Lipid Membranes*, edited by C. R. Safinya and J. O. Raedler (Taylor & Francis, 2021).
- [23] E. Spruijt, J. Sprakel, M. A. Cohen Stuart, and J. van der Gucht, Interfacial tension between a complex coacervate phase and its coexisting aqueous phase, *Soft Matter* **6**, 172 (2010).
- [24] P. R. Banerjee, A. N. Milin, M. M. Moosa, P. L. Onuchic, and A. A. Deniz, Reentrant phase transition drives dynamic substructure formation in ribonucleoprotein droplets, *Angew. Chem. Int. Ed.* **56**, 11354 (2017).
- [25] I. Alshareedah, G. M. Thurston, and P. R. Banerjee, Quantifying viscosity and surface tension of multicomponent protein-nucleic acid condensates, *Biophys. J.* **120**, 1161 (2021).
- [26] T. J. Welsh, G. Krainer, J. R. Espinosa, J. A. Joseph, A. Sridhar, M. Jahnel, W. E. Arter, K. L. Saar, S. Alberti, R. Collepardo-Guevara, and T. P. J. Knowles, Surface electrostatics govern the emulsion stability of biomolecular condensates, *Nano Lett.* **22**, 612 (2022).
- [27] A. Agrawal, J. F. Douglas, M. Tirrell, and A. Karim, Manipulation of coacervate droplets with an electric field, *Proc. Natl. Acad. Sci. U.S.A.* **119**, e2203483119 (2022).
- [28] M. Vis, V. F. D. Peters, E. M. Blokhuis, H. N. W. Lekkerkerker, B. H. Ern e, and R. H. Tromp, Decreased interfacial tension of demixed aqueous polymer solutions due to charge, *Phys. Rev. Lett.* **115**, 078303 (2015).
- [29] O. Adame-Arana, C. A. Weber, V. Ziburdaev, J. Prost, and F. Jülicher, Liquid phase separation controlled by pH, *Biophys. J.* **119**, 1590 (2020).
- [30] A. Majee, M. Bier, R. Blosssey, and R. Podgornik, Charge symmetry broken complex coacervation, *Phys. Rev. Research* **2**, 043417 (2020).
- [31] J. R. Casey, S. Grinstein, and J. Orlowski, Sensors and regulators of intracellular pH, *Nat. Rev. Mol. Cell Biol.* **11**, 50 (2010).
- [32] A. Kurotani, A. A. Tokmakov, K.-I. Sato, V. E. Stefanov, Y. Yamada, and T. Sakurai, Localization-specific distributions of protein pi in human proteome are governed by local pH and membrane charge, *BMC Mol. Cell Biol.* **20**, 36 (2019).
- [33] A. J. Bray, Theory of phase-ordering kinetics, *Adv. Phys.* **51**, 481 (2002).
- [34] C. A. Weber, D. Zwicker, F. Jülicher, and C. F. Lee, Physics of active emulsions, *Rep. Prog. Phys.* **82**, 064601 (2019).
- [35] V. S. Bagotsky, *Fundamentals of Electrochemistry*, 3rd ed. (Wiley, Hoboken, NJ, 2006).
- [36] M. Vis, V. F. D. Peters, R. H. Tromp, and B. H. Ern e, Donnan potentials in aqueous phase-separated polymer mixtures, *Langmuir* **30**, 5755 (2014).
- [37] J. N. Israelachvili, *Intermolecular and Surface Forces* (Academic Press, Amsterdam, 2011).
- [38] L. Leibler, Theory of microphase separation in block copolymers, *Macromolecules* **13**, 1602 (1980).
- [39] L. Leibler, Block copolymers at interfaces, *Physica A* **172**, 258 (1991).
- [40] J. Wittmer and J. Joanny, Charged diblock copolymers at interfaces, *Macromolecules* **26**, 2691 (1993).
- [41] M. Bier, A. Gambassi, and S. Dietrich, Local theory for ions in binary liquid mixtures, *J. Chem. Phys.* **137**, 034504 (2012).
- [42] N. Gavish and A. Yochelis, Theory of phase separation and polarization for pure ionic liquids, *J. Phys. Chem. Lett.* **7**, 1121 (2016).
- [43] R. Kjellander and D. Mitchell, An exact but linear and Poisson-Boltzmann-like theory for electrolytes and colloid dispersions in the primitive model, *Chem. Phys. Lett.* **200**, 76 (1992).
- [44] P. Attard, Asymptotic analysis of primitive model electrolytes and the electrical double layer, *Phys. Rev. E* **48**, 3604 (1993).
- [45] R. L. de Carvalho and R. Evans, The decay of correlations in ionic fluids, *Mol. Phys.* **83**, 619 (1994).
- [46] A. M. Smith, A. A. Lee, and S. Perkin, The electrostatic screening length in concentrated electrolytes increases with concentration, *J. Phys. Chem. Lett.* **7**, 2157 (2016).

- [47] H. Nikaido, Porins and specific channels of bacterial outer membranes, *Mol. Microbiol.* **6**, 435 (1992).
- [48] G. M. Geise, H. J. Cassady, D. R. Paul, B. E. Logan, and M. A. Hickner, Specific ion effects on membrane potential and the permselectivity of ion exchange membranes, *Phys. Chem. Chem. Phys.* **16**, 21673 (2014).
- [49] K. K. Nakashima, M. H. van Haren, A. A. André, I. Robu, and E. Spruijt, Active coacervate droplets are protocells that grow and resist Ostwald ripening, *Nat. Commun.* **12**, 3819 (2021).
- [50] S. Chen and Z.-G. Wang, Charge asymmetry suppresses coarsening dynamics in polyelectrolyte complex coacervation (2023), [arXiv:2308.16334 \[cond-mat.soft\]](https://arxiv.org/abs/2308.16334).
- [51] M. Tena-Solsona, J. Janssen, C. Wanzke, F. Schnitter, H. Park, B. Rieß, J. M. Gibbs, C. A. Weber, and J. Boekhoven, Accelerated ripening in chemically fueled emulsions, *ChemSystemsChem* **3**, e2000034 (2021).
- [52] T.-Y. D. Tang, M. Antognozzi, J. A. Vicary, A. W. Perriman, and S. Mann, Small-molecule uptake in membrane-free peptide/nucleotide protocells, *Soft Matter* **9**, 7647 (2013).
- [53] B. Ghosh, R. Bose, and T. D. Tang, Can coacervation unify disparate hypotheses in the origin of cellular life?, *Curr. Opin. Colloid Interface Sci.* **52**, 101415 (2021).
- [54] R. Kubota, S. Torigoe, and I. Hamachi, Temporal stimulus patterns drive differentiation of a synthetic dipeptide-based coacervate, *J. Am. Chem. Soc.* **144**, 15155 (2022).
- [55] J. Bauermann, G. Bartolucci, J. Boekhoven, C. A. Weber, and F. Jülicher, Formation of liquid shells in active droplet systems (2023), [arXiv:2306.10852 \[cond-mat.soft\]](https://arxiv.org/abs/2306.10852).
- [56] A. M. Bergmann, J. Bauermann, G. Bartolucci, C. Donau, M. Stasi, A.-L. Holtmannspoetter, F. Jülicher, C. A. Weber, and J. Boekhoven, Liquid spherical shells are a non-equilibrium steady state, *bioRxiv* [10.1101/2023.01.31.526480](https://doi.org/10.1101/2023.01.31.526480) (2023).